Advances in Nanoparticles, 2022, 11, 111-128
https://www.scirp.org/journal/anp
ISSN Online: 2169-0529
ISSN Print: 2169-0510

Study of Photocatalytic Activity of a Nanostructured Composite of ZnS and Carbon Dots

Irié Bi Irié Williams[1], Essy Kouadio Fodjo[1*], Pomi Bi Boussou Narcisse[1], Aka Alla Martin[1], Koffi Koffi Kra Sylvestre[1], Trokourey Albert[1], Zhen Gu[2*]

[1]Laboratory of Constitution and Reaction of Matter, UFR SSMT, Université Felix Houphouet Boigny, Abidjan, Cote d'Ivoire
[2]Key Laboratory of Advanced Control and Optimization for Chemical Processes Ministry of Education, East China University of Science and Technology, Shanghai, China
Email: *kouadio.essy@univ-fhb.edu.ci, *guzhen@ecust.edu.cn

How to cite this paper: Williams, I.B.I., Fodjo, E.K., Narcisse, P.B.B., Martin, A.A., Sylvestre, K.K.K., Albert, T. and Gu, Z. (2022) Study of Photocatalytic Activity of a Nanostructured Composite of ZnS and Carbon Dots. *Advances in Nanoparticles*, **11**, 111-128.
https://doi.org/10.4236/anp.2022.114007

Received: August 2, 2022
Accepted: November 19, 2022
Published: November 22, 2022

Abstract

Environmental pollution jeopardizes our existence. For this purpose, research is moving more and more towards the search for economic means and green chemistry to curb this phenomenon. In this context, the photocatalytic activity of zinc sulfide nanoparticles (ZnS NPs) and nanostructured composite ZnS/carbon dots (ZnS/CDs) was evaluated after their synthesis. The results of X-ray diffraction (XRD) analysis indicate that the crystal structure of ZnS/CDs is identical to that of the cubic phase structure of ZnS, revealing that the cubic phase structure of ZnS was not altered in the presence of CDs. Indeed, there is no additional peak in the crystal structure of ZnS/CDs, revealing that the crystalline structure of ZnS is not responsible for the difference in photocatalytic activity between ZnS/CDs and ZnS NPs. Moreover, analysis performed by transmission electron microscopy (TEM) shows aggregation of the synthesized ZnS and ZnS/CDs nanoparticles with an average size estimated around 10 nm and 12 nm, respectively. In addition, the reflectance study in the visible range shows a reduction in the sunlight reflection intensity using ZnS/CDs compared to the capability of ZnS NPs. Photocatalytic degradation tests reveal that ZnS/CDs have the best methylene blue (MB) degradation rate. Indeed, under the optimal conditions, the photocatalytic activity can reach 100% efficiency within 100 min and 240 min of sunlight exposure for the degradation of 7.5 mg/L MB using ZnS/CDs and ZnS, respectively. This improvement in photocatalytic activity of ZnS/CDs may be due to the presence of CDs which can permit to undergo a reduction of reflection properties of ZnS NPs in the visible range. These results show that CDs can play a key role in enhancing the photocatalytic activity of ZnS, and suggest that ZnS/CDs could be used as

eco-friendly composite materials for the degradation of organic pollutants of similar structures in the aquatic environment under solar irradiation.

Keywords

Fluorescent Carbon Dots (CDs), Photocatalytic Degradation of Methylene Blue, Sunlight Reflectance Property, Synthesis of ZnS Nanoparticles

1. Introduction

Owing to their activities, factories namely textile, tanning and printing industries release dyes into the environment which pose a real environmental problem [1]. These dyes are considered as pollutants and constitute a major threat for all aquatic life because they can reduce light rays in the aquatic environment, thus blocking the phenomenon of photosynthesis [1] [2] [3]. The treatment of these wastes remains a major challenge to integrate sustainable development concepts. It is therefore important to develop robust, cost-effective, efficient and environmentally friendly technologies for the degradation of these dyes before their release into the environment [4] [5]. In most cases, the conventional waste treatments have the disadvantage of transferring the pollution from an aqueous phase to a new phase, which leads to a concentrated sludge, creating a secondary waste problem or generating materials that are often very expensive. In this perspective, semiconductor nanostructures have been the subject of hotspot of research. Indeed, semiconductor with particular designed nanostructure features is of great importance owing to their unique properties which considerably differ from the same materials in bulk state [6]. Semiconductor nanostructures, in particular those of groups II - VI, have attracted great interest due to their exceptional optical and electronic properties which arise from the surface-to-volume ratio and the quantum confinement effect [7]. Among the semiconductor nanostructures, zinc sulfide (ZnS) with a wide band gap (3.72 eV for the cubic phase and 3.77 eV for the hexagonal wurtzite phase) [6] [8], has been a subject of investigation because of their fundamental properties for various applications such as photovoltaic [9], and photocatalysis [10] [11]. Moreover, the nanoparticles of ZnS (ZnS NPs) have been shown to be one of the richest types among all inorganic semiconductor photocatalysts. ZnS NPs have an optical transparency from ultraviolet (UV) to infrared (IR) and good chemical stability with many advantages, among others, they have excellent transport properties (reduced carrier dispersion and recombination), good stability, high electron mobility, and they are non-toxic and relatively low cost [6]. Furthermore, considerable attempts have been made to develop light-driven ZnS photocatalysts using less energy ($\lambda \geq 420$ nm), which is more abundant [12]. Many major issues to achieve high photocatalytic efficiency are due to light absorption and rapid recombination of electron-hole pairs [13]. Thus, improving charge separation and light absorption is crucial for

enhancing photocatalytic performance [14] [15].

With the growing concerns about environmental pollution and energy crisis, the importance of the nanostructured semiconductor materials has been reported, particularly, their application in photodegradation of organic pollutants [16]. Despite the above-mentioned limitations, the absorption wavelength can be adjusted to higher wavelength by doping these ZnS NPs using appropriate nanomaterials [2]. Over the past few decades, carbon dots (CDs) have experienced remarkable growth due to their optical performance and electronic properties, as well as their excellent biocompatibility, high aqueous solubility, and low toxicity. These impeccable properties make them ideal candidates for their applications in the fields such as biomedical, optoelectronics and photocatalysis.

In this study, CDs were prepared by a green method in our previous work via chemical fragmentation. Charcoal was used as a carbon source to fabricate a ZnS/CDs nanocomposite [17]. Indeed, combining ZnS with CDs as one nanostructure promotes photogenerated electrons from the valence band to the conduction band by reducing its band gap, preventing electron and hole recombination. Evaluation of the photocatalytic efficiency for the degradation of methylene blue (MB) has shown that the synthesized ZnS/CDs have twofold higher rate compared to that of ZnS NPs. This excellent efficiency could be due to the reduction of reflective properties of ZnS NPs especially the shift towards the visible range of their absorption wavelength in the presence of CDs. This enhancement of the photocatalytic properties of ZnS NPs using CDs may offer an innovative approach to produce very efficient photocatalysts.

2. Materials and Methods

2.1. Reagents

In this study, all chemicals are commercially available and are used without further purification. Zinc nitrate hexahydrate ($(Zn(NO_3)_2, 6H_2O)$, 98%,) and ammonium hydroxide (NH_4OH, 28% - 30%) were supplied by Honeywell Fluka (Buchs, Switzerland). Methylene blue ($C_{16}H_{18}ClN_3S$, 98%) was purchased from Merck (Darmstadt, Germany). Ethanol (C_2H_5OH, 98%), hydrochloric acid (HCl, 37%), acetone (C_3H_6O, 98%), and potassium hydroxide (KOH, 85%) were supplied by Panreac quimica (Barcelona, Spain). Sodium sulfide (Na_2S) was purchased from Sigma Aldrich (St. Louis, MO, USA). Deionized (DI) water used in this study was produced by water purification system Sichuan Zhuoyue Water Treatment Equipment CO., Ltd. (Chengdu, China). The water purification system can allow obtaining DI water with resistivity of 18.25 MWžcm. The charcoal used to prepare the CDs was obtained from the local market (Abidjan, Ivory Coast).

2.2. Synthesis of CDs, ZnS NPs and ZnS/CDs Nanocomposites

The CDs were prepared according to the procedure described in the literature using chemical fragmentation method at a relatively low temperature (50˚C). In

a typical synthesis procedure as described in our previous work [17], 50 mL of 2.5 M NH_4OH solution was prepared from commercial NH_4OH by dilution with DI water. Afterwards, 500 mg of the powdered charcoal was added to this solution at previously adjusted temperature of 50˚C in a water bath under a magnetic stirring at 500 rpm for 10 min and under fume hood, followed by gentle stirring at the same temperature (50˚C) for 12 h. The resulting solution was then cooled to room temperature and centrifuged at 4000 rpm for 5 min using a high-speed benchtop centrifuge (MRC Ltd., Holon, Israel) to remove the macroparticles. To the recovered supernatant, DI water was added to reach 25 mL. The newly obtained solution was heated again at 50˚C in the water bath under stirring at 500 rpm for 10 min. To this solution, 17 mL of 2.5 M NH_4OH solution was added and the solution was filled with DI water to reach a final volume of 50 mL. This new solution was kept at 50˚C with gentle stirring for 12 h. The solution was cooled to room temperature and then centrifuged at 4000 rpm for 5 min to finally obtain the suspension of CDs.

ZnS nanostructures were synthesized by the precipitation method using zinc nitrate ($Zn(NO_3)_2$, $6H_2O$) and sodium sulfide (Na_2S) as precursors [18]. First of all, 0.891 g of zinc nitrate was dissolved in 50 mL of deionized water and 2.760 g of Na_2S in another 50 mL of deionized water. Both solutions were kept under constant stirring for 30 min for their complete dissolution. Then, the Na_2S solution was added dropwise to the zinc nitrate solution at room temperature (28˚C) under vigorous stirring at 500 rpm for 3 h to obtain the formation of a white precipitate. The resulting product was centrifuged and washed with DI water and ethanol, and then calcined in air at 400˚C for 3 h with a temperature rise of 5˚C/min.

The nanocomposite consisting of CDs and ZnS NPs (ZnS/CDs) was synthesized according to the previously described procedure [19]. Briefly, 250 mg of synthesized ZnS NPs was dispersed in 125 mL of ethanol and vortexed for 10 min. To this solution, 50 µL of the prepared colloidal solution of CDs was added. This mixture was stirred at 500 rpm for 30 min at room temperature. The obtained solution was collected by centrifugation, washed three times with ethanol, and dried at 100˚C for 3 h to finally obtain the ZnS/CDs nanocomposites.

2.3. Characterization of the Synthesized Nanostructures

X-ray diffraction (XRD) analysis of the different prepared samples was performed using Siemens D5005 diffractometer (Simens AG, Munich, Germany) with a copper anticathode ($\lambda K\alpha 1$ = 1.5406 Å). The angle of incidence 2Θ varied from 5˚C to 90˚C, with a step size of 0.02. The absorbance and reflectance of these samples were measured with Flame-S-XR1 UV-Vis spectrometer (Ocean Optics, Largo, USA). Fluorescence test of the synthesized CDs was done using Qiwei WFH-204B 254/365 nm portable UV lamp (Hangzhou, China). Size characterization of ZnS NPs and ZnS/CDs was performed by Transmission electron microscopy (MET) using a JEOL JEM-2010 apparatus (Tokyo, Japan).

2.4. Photocatalytic Analysis

In this study, all photocatalytic experiments were performed between 11:00 AM and 3:00 PM in order to take maximum advantage of the solar irradiation as for this range of the time, the sunlight is very intense. To evaluate the photocatalytic properties of ZnS and ZnS/CDs nanostructures, 300 mg of ZnS NPs (or ZnS/CDs) were introduced into a beaker containing 100 mL of 7.5 mg/L MB, which is chosen as model of pollutant. This mixture was kept in the dark under magnetic stirring at 500 rpm for 30 min to reach adsorption-desorption equilibrium [20]. Once equilibrium was reached, the mixture was exposed to sunlight at different times. Under the sun irradiation, 2 mL samples were taken every 30 and 20 min for MB alone or contaminated with wastewater, respectively, and finally centrifuged. The remaining MB concentration in the centrifuged solutions were analyzed by measuring the absorbance peak at 664 nm (characteristic peak of MB) using the UV-Vis spectrophotometer. Then, the calculation of the percentage of dye degradation in the presence of ZnS NPs or ZnS/CDs was evaluated using Equation (1):

$$\%D = \frac{C_0 - C_t}{C_0} \times 100 \tag{1}$$

where C_0 represents the initial concentration of the MB dye and C_t its concentration after solar irradiation at a time t.

This procedure was used for the study of the influence of the initial concentration of MB, catalyst mass and the pH of the media on the degradation of MB by varying the initial concentration of MB from 5 mg/L to 15 mg/L, the mass of ZnS NPs from 100 mg to 350 mg and the pH of the media from 2 to 13, respectively.

2.5. Kinetic Study of MB Degradation

To know the kinetic order of the MB degradation reaction, the kinetic study of the photocatalytic reaction of MB was carried out by varying the initial concentration of MB from 5 to 15 mg/L (5 mg/L, 7.5 mg/L, 10 mg/L, 12.5 mg/L and 15 mg/L). In detail, a mass of 300 mg of ZnS NPs or ZnS/CDs was added to 100 mL of MB solution at the above different concentrations. The kinetic order of MB dye degradation is evaluated using Equations (2) and (3) [21]:

- Pseudo-first order kinetics equation:

$$\ln\left(\frac{C_0}{C_t}\right) = k_1 t \tag{2}$$

- Pseudo-second order equation can be formulated as displayed in Equation (3):

$$\frac{1}{C_t} - \frac{1}{C_0} = k_2 t \tag{3}$$

where C_0 and C_t are the initial and different time t concentration of MB, respectively. k_1 and k_2 are the rate constants for the pseudo-first-order and pseu-

do-second-order models, respectively.

The study of MB adsorption isotherms on ZnS NPs and ZnS/CDs was performed for the following models:

- Langmuir-Hinshelwood model: Langmuir-Hinshelwood model is widely used to describe the experimental results in heterogeneous photocatalysis. This model is expressed by Equation (2).
- Temkin model: Temkin isotherm accounts for the fact that the heat of adsorption of all molecules in the covering layer decreases linearly with covering due to the decrease in adsorbent-adsorbate interactions. The adsorption is characterized by a uniform distribution of surface binding energies. Temkin isotherm is expressed according to Equation (4) [22]:

$$q_e = B_1 \cdot \ln K_t + B_1 \cdot \ln C_e \tag{4}$$

with B_1 the Temkin constant, K_t ($L \cdot g^{-1}$), the adsorption equilibrium constant corresponding to the maximum binding energy, and C_e (mg/L^{-1}) the equilibrium concentration of adsorbate.

2.6. Application

In order to evaluate the applicability of the photocatalytic properties of the synthesized ZnS NPs and ZnS/CDs in a real sample, wastewater from the University Hospital of Cocody (UHC) was examined by its contamination or not with MB. The wastewater samples were collected from UHC and then transferred to a one-liter polyethylene canister, stored at 4˚C, and protected from light in a cooler containing ice to avoid possible photochemical reactions. The samples were then transported to the laboratory and stored in a refrigerator at 4˚C. Processing in the laboratory was performed as soon as possible. Before any measurements, the wastewater samples were decanted and filtered through a 0.45 µm diameter FILTER LAB filter. It should be noted that the collected water is yellow in color with a temperature of 27.6˚C, pH of 8.4, conductivity of 836 µS/cm, and water salinity of 1.7.

3. Results and Discussion

3.1. Characterization of the Synthesized Nanostructures

To confirm that CDs were synthesized from charcoal, the characterization of the synthesized product was performed using UV-Vis and TEM (**Figure 1(a)** and **Figure 1(b)**). As shown in **Figure 1(a)**, the adsorption spectrum of the CDs displays an intense peak around 226 nm with a characteristic shoulder around 270 nm. This observed peak around 226 nm can be attributed to the π-π* transition of C=C bonds, while the shoulder is attributed to the n-π transition of C-O, suggesting that CDs with terminations rich in carboxylic, carbonyl, and alcohol functional groups were synthesized [23] [24]. Furthermore, the TEM image (**Figure 1(b)**) shows that the synthesized particles are around 4 nm as average size, indicating that CDs are synthesized from the charcoal.

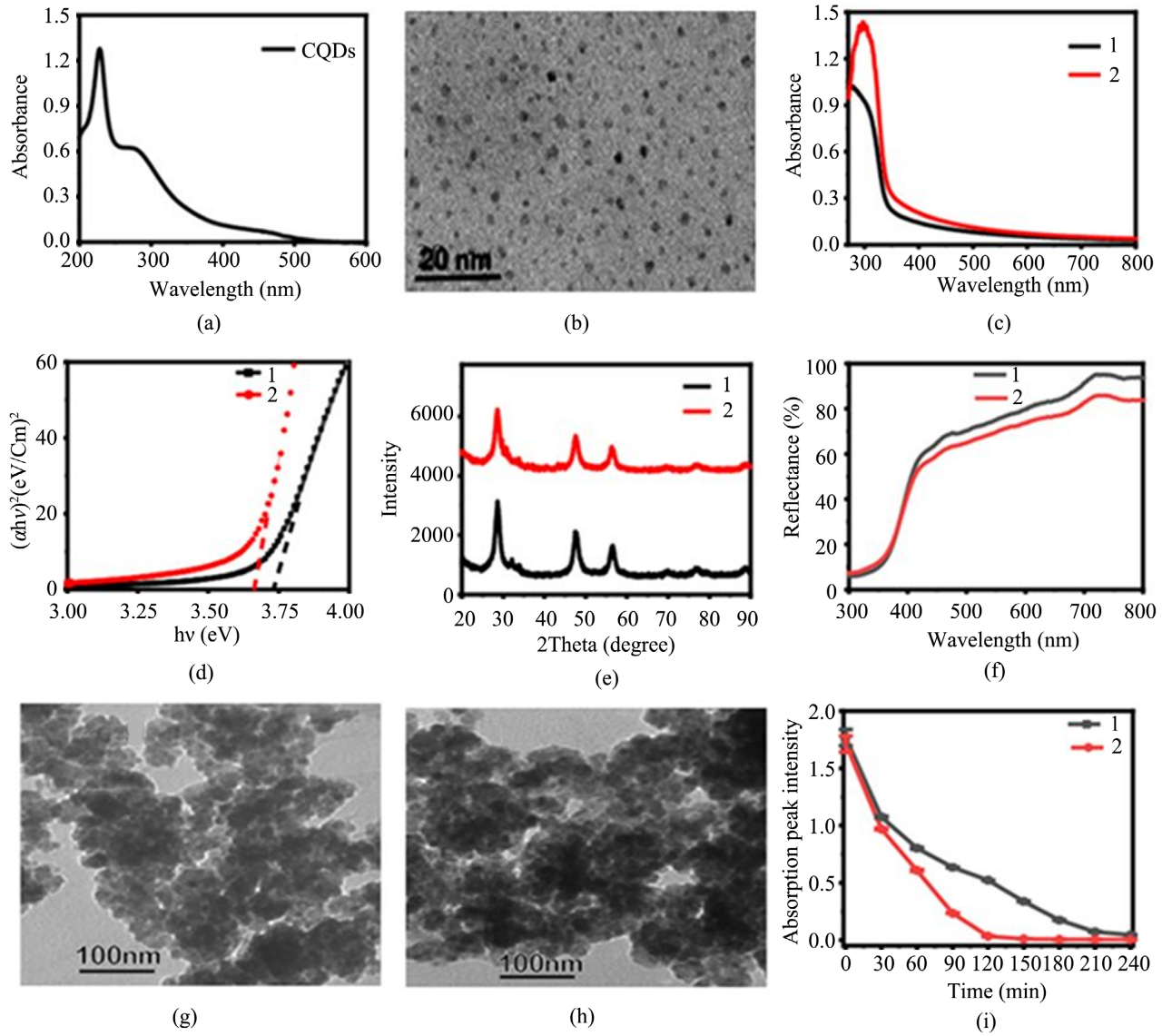

Figure 1. (a) UV-Vis spectrum and (b) TEM image of CDs, (c) UV-Vis spectra and (d) plot of $(\alpha h\nu)^2$ vs hν of ZnS NPs (1) and ZnS/CDs (2). (e) XRD spectra and (f) reflectance spectra of ZnS NPs (1) and ZnS/CDs (2). TEM images of (g) ZnS NPs and (h) ZnS/CDs. (i) Degradation of 7.5 mg/L MB under solar irradiation using ZnS NPs (1) and ZnS/CDs (2) as photocatalysts.

Moreover, in order to study the optical effect of the nanostructured composite of ZnS/CDs, the measurement of the UV-Vis spectrum and band gap energy of ZnS and ZnS/CDs were evaluated (**Figure 1(c)** and **Figure 1(d)**). As displayed in **Figure 1(c)**, the maximum absorption peak of ZnS/CDs is red-shift compared with the maximum of ZnS NPs one, which both appeared between 300 and 400 nm. These results clearly indicate that, though both nanostructures can absorb light in the visible range, ZnS/CDs absorb more, suggesting that the presence of CDs promotes good absorption of visible light by ZnS NPs. This visible light absorption by ZnS/CDs nanocomposites could promote better photocatalytic activity of this latter. In addition, the band gap energy (*Eg*) (**Figure 1(d)**) evaluated using Tauc relation (Equation (5)), gives 3.7 eV and 3.5 eV for ZnS NPs and

ZnS/CDs, respectively.

$$(\alpha h\upsilon)^2 = B(h\upsilon - Eg) \tag{5}$$

where h is Planck's constant, υ is the frequency, Eg the band gap energy of the semiconductor, B proportional constant, and α is the absorption coefficient evaluated using Equation (6) [25]:

$$\alpha = \frac{2.303A}{l} \tag{6}$$

with l = 1 cm, the optical path length corresponding to the thickness of the measurement cell and A, the absorbance.

These results confirm that the addition of CDs can promote ZnS NPs to have better absorptive capacity of visible light. However, the decrease in the band gap energy after the addition of CDs can be attributed to intrinsic states and interfaces that produce confined electronic levels in the band gap. This effect can lead to the enhancement of the photocatalytic properties of ZnS/CDs [20].

Besides, effect of the nanostructured composite of ZnS/CDs was investigated using XRD technique (**Figure 1(e)**). The obtained diffraction peaks at (111), (220), and (311) reflection planes observed at 2θ of 29.04˚, 48.06˚, and 57.11˚, respectively, can be attributed to cubic phase of zinc-blende structure according to JCPDS data sheet No. 05-0566 [26]. Moreover, no additional characteristic peak of CDs could be observed, suggesting that CDs may have relatively low content in ZnS. The obtained results may clearly show also that the presence of CDs does not affect the crystalline structure of ZnS NPs [20].

However, the slight decrease in the intensity of the diffraction peaks of the different ZnS/CDs peaks indicates that ZnS NPs have higher crystalline structure than ZnS/CDs. Importantly, size around 10 nm and 12 nm for ZnS NPs and ZnS/CDs, respectively, were determined using the Debye-Scherrer equation (Equation (7)):

$$D_{hkl} = \frac{0.9\lambda}{\beta_{hkl}\cos\theta_{hkl}} \tag{7}$$

where D_{hkl} (nm) is the grain size; λ is the wavelength of the X-ray beam; θ_{hkl} is the diffraction angle; and β_{hkl} is the half-value width expressed in radians for hkl.

Additionally, optical properties of ZnS NPs and ZnS/CDs were evaluated measuring their reflectance in UV-Vis range (**Figure 1(f)**). The obtained results show that the reflectance of ZnS NPs is significantly higher than that of ZnS/CDs nanocomposites in the visible range, indicating that the nanostructured composite of ZnS/CDs displays a significant reduction in the reflection of light rays by ZnS NPs in the visible range. Therefore, the photocatalytic efficiency of ZnS/CDs could be better than that of ZnS NPs under visible light irradiation [27].

However, to confirm the size of the synthesized nanomaterials, the characterization of the prepared materials was performed using TEM (**Figure 1(g)** and **Figure 1(h)**). The results indicate that both ZnS and ZnS/CDs are polydisperse nanomaterials. These different sizes could play an important role in their pho-

tocatalytic application.

3.2. Study of the Photocatalytic Properties of the Synthesized Nanostructures

3.2.1. MB Degradation Using the Synthesized Nanostructures as Catalyst under Solar Irradiation

In order to avoid pollution of the environment, especially natural resources such as soil and water, it is necessary to develop effective treatment methods to remove the pollutants from these media. For this purpose, the photocatalytic properties of ZnS NPs and ZnS/CDs for the removal of MB under solar irradiation at room temperature were evaluated in aqueous media (**Figure 1(i)**). The absorbance peak intensity of MB at the wavelength of 664 nm decreases with time and almost disappears after 100 min of irradiation using ZnS/CDs while it will take more than 240 min of sun irradiation to obtain the same result in the presence of ZnS NPs. This disappearance of the peak indicates the degradation of MB by ZnS NPs and ZnS/CDs, showing the excellent photocatalytic efficiencies of ZnS NPs and ZnS/CDs for the degradation of MB in aqueous environment [20]. However, the higher photocatalytic efficiency of ZnS/CDs could be due to the shift of their maximum absorbance peak to visible range after the addition of CDs.

3.2.2. Influence of Initial MB Concentration on MB Degradation Rate

To highlight the influence of the initial concentration on the rate of degradation of MB, five experiments with different initial concentrations between 5 and 15 mg/L of MB were performed. The results (**Figure 2(a)** and **Figure 2(b)**) show that the rate of MB degradation decreases with increasing initial concentration. These results are in good agreement with the literature [28] [29]. This evolution can be attributed to the formation of several layers of MB adsorbed on the surface of the photocatalyst thus making the sites of the photocatalyst inaccessible to photons or the absorption of light by the molecules of MB, consequently reducing the number of photons reaching the surface of the photocatalyst.

3.2.3. Influence of ZnS NPs Mass on MB Degradation

In photocatalytic processes, the mass of the catalyst is an important parameter that can affect the degradation rate. In order to evaluate the optimal mass of the photocatalyst upon removal of the MB dye, a series of experiments were performed by varying the mass of photocatalyst (ZnS NPs) from 100 to 350 mg under sunlight. The results in **Figure 2(c)** show that the MB degradation increases with the increasing of photocatalyst mass until 300 mg and decrease beyond, suggesting that 300 mg is the optimal mass. However, for a mass higher than 300 mg, the lower efficiency could be explained by the turbidity of the solution, thus reducing the efficiency of the catalytic reaction while in the case of a small amount of catalyst, the MB molecules can prevent the solar from reaching the catalyst surface [17]. At 300 mg, a large number of sites are activated, leading to

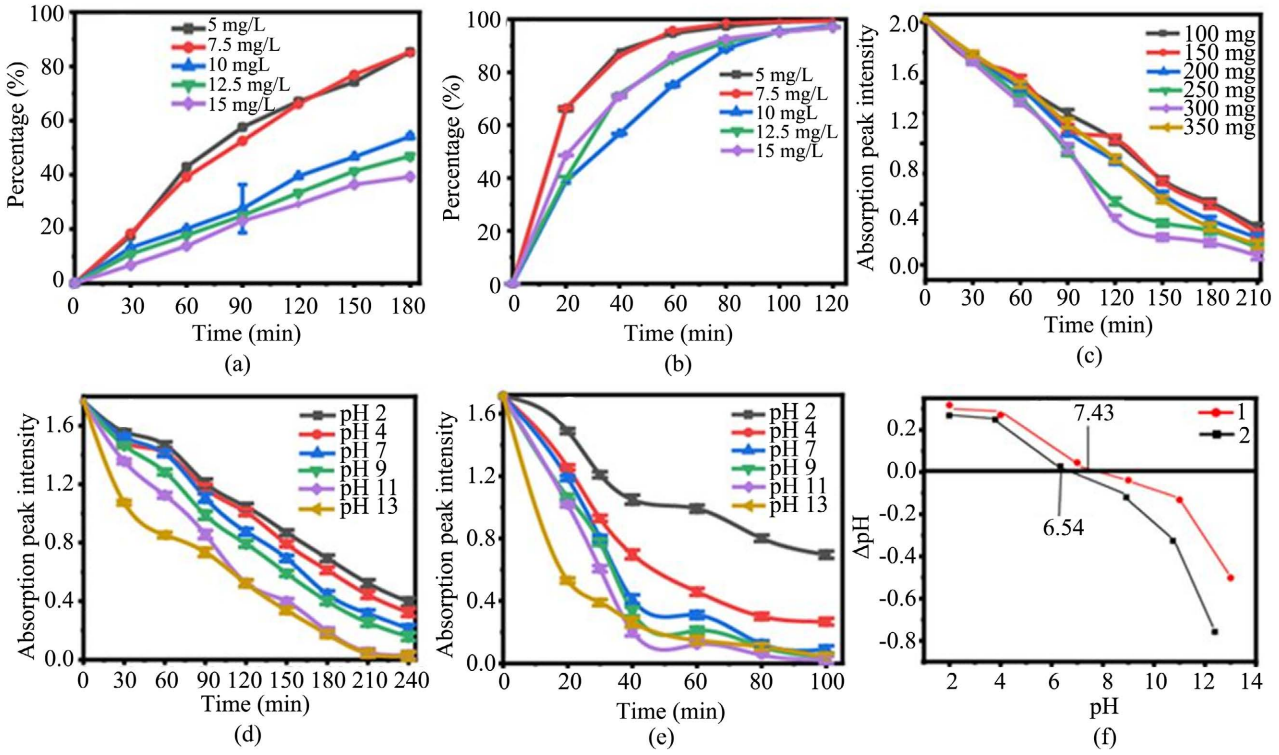

Figure 2. Percentage of removed MB at different times with (a) ZnS NPs and (b) ZnS/CDs. (c) MB degradation (7.5 mg/L) for different masses of ZnS NPs at different times. Effect of pH with (d) ZnS NPs and (e) ZnS/CDs as photocatalysts on the degradation of 7.5 mg/L MB, and (f) pH variation as a function of the initial pH of ZnS (1) and ZnS/CDs (2).

an important production of free hydroxyl radicals (●OH) in the medium, allowing therefore the degradation of MB.

3.2.4. Influence of pH on the MB Degradation

The pH is a parameter which can affect the surface properties of the solids, and characterize the medium in which the pollutants should be removed. Its effect on the photocatalytic activity must therefore be studied in the case of water loaded with pollutant. Indeed, the dispersion of the particles and the surface charge of the catalyst are influenced by the pH. To evaluate the effect of pH on the degradation efficiency of MB, experiments were performed at different pH, ranging from 2 to 13 for an initial dye concentration of 7.5 mg/L under sunlight (**Figure 2(d)** and **Figure 2(e)**). As can be seen from these figures, MB degradation increases with increasing pH in the presence of ZnS NPs or ZnS/CDs. The best degradation (100%) was obtained from pH 11 after 240 min and 100 min of solar irradiation for ZnS NPs and ZnS/CDs, respectively. This result could be understood by the fact that MB is cationic. This positive charge on MB results in weak adsorption on the photocatalyst surface in acidic medium due to the repulsion forces between the positive catalyst surface and the positive charge of MB. The higher MB degradation efficiency obtained at pH = 11 is attributed to the attractive electrostatic interactions between the negative catalyst surface and the positive charge of the cationic MB. The presence of large amounts of OH^- ions

on the catalyst surface as well as in the reaction medium favors the formation of ●OH radicals, which are widely known as the main oxidizing species responsible for the degradation process [29].

In order to understand this pH effect, the point of zero charge (PZC) was evaluated for each nanostructure (ZnS NPs and ZnS/CDs). To achieve this goal, the suspensions of each catalyst were subjected to a zero charge moisture test. Indeed, 20 mg of ZnS NPs or ZnS/CDs were dissolved in 20 mL of an aqueous solution of 0.1 M KNO_3 and adjusted to different pH ranging from 2 to 13. The suspension was shaken over 24 h at room temperature and the final pH of the solutions was measured. The difference between the final pH and the initial pH (ΔpH) was plotted as a function of the initial pH of the solution (**Figure 2(f)**). The intersection of this curve with the abscissa axis corresponds to the PZC (pHpzc) [30]. The obtained results show that the pHpzc for ZnS and ZnS/CDs are around 7.4 and 6.5, respectively. These pHpzc suggest that the high performance of these nanostructures as photocatalysts should be good in alkaline media for pollutant with positive charge, confirming the above results. It should be noted that the presence of CDs has slightly broadened the pH range from the range 7.4 - 14 to the range 6.5 - 14 for the removal of cationic pollutants, at the same time it can be seen that their presence has reduced the pH range for the degradation activity of the anionic pollutants. Indeed, these results can be explained by the reaction mechanism as displayed in Equations (8)-(15). When visible light falls on the surface of ZnS NPs, electrons are excited from the valence band (VB) of ZnS NPs to their conduction band (CB), leaving behind holes on the valence band. Usually, these photogenerated electrons and holes quickly recombine and only a few charge carriers remain to participate in the reaction. This leaves only a few charge carriers that take part in the photocatalytic system. However, upon addition of the CDs to ZnS NPs, the electrons from the ZnS CB are transferred to the CDs, resulting in an efficient separation of the light-generated electron and hole pairs. This separation enhances the photocatalytic performance of the nanocomposite. Ultimately, these photogenerated electrons react with the absorbed oxygen forming superoxide radical anions. Afterwards, the photogenerated holes in the ZnS VB react with the hydroxyl ions in the aqueous solution to generate highly reactive hydroxyl radicals. These hydroxyl radicals underwent combination to form hydrogen peroxide, which in turn can react with the superoxide radical anions to produce more hydroxyl radicals which are the main source of the degradation of MB as explained in Equations (8) to (15) [20].

$$\mathrm{ZnS} + \mathrm{h}\vartheta \rightarrow \mathrm{e}^{-}\left(\mathrm{CB}\right) + \mathrm{h}^{+}\left(\mathrm{VB}\right) \tag{8}$$

or

$$\mathrm{ZnS/CQDs} + \mathrm{h}\vartheta \rightarrow \mathrm{e}^{-}\left(\mathrm{CB}\right) + \mathrm{h}^{+}\left(\mathrm{VB}\right) \tag{9}$$

$$\mathrm{e}^{-}\left(\mathrm{CB}\right) \rightarrow \mathrm{e}^{-}\left(\mathrm{CQDs}\right) \tag{10}$$

$$\mathrm{e}^{-}\left(\mathrm{CQDs}\right) + \mathrm{O}_2 \rightarrow \mathrm{O}_2^{\bullet -} \tag{11}$$

$$h^{+}(VB) + H_2O \rightarrow H^{+} + \bullet OH \quad (12)$$

$$2HO^{\bullet} \rightarrow H_2O_2 \quad (13)$$

$$H_2O_2 + O_2^{\bullet -} \rightarrow OH^{\bullet} + OH^{-} + O_2 \quad (14)$$

$$MB + OH^{\bullet}/OH^{-} \rightarrow CO_2 + H_2O \quad (15)$$

3.2.5. Kinetics of MB Degradation

The establishment of kinetics relating to a reaction mechanism is based globally on the study of the effect of the initial concentration of the substrate. The kinetics of MB degradation in the presence of ZnS NPs and ZnS/CDs were carried out. The values of photodegradation kinetic constants of MB are determined using Equations (2) and (3) for pseudo first order (**Figure 3(a)** and **Figure 3(b)**)

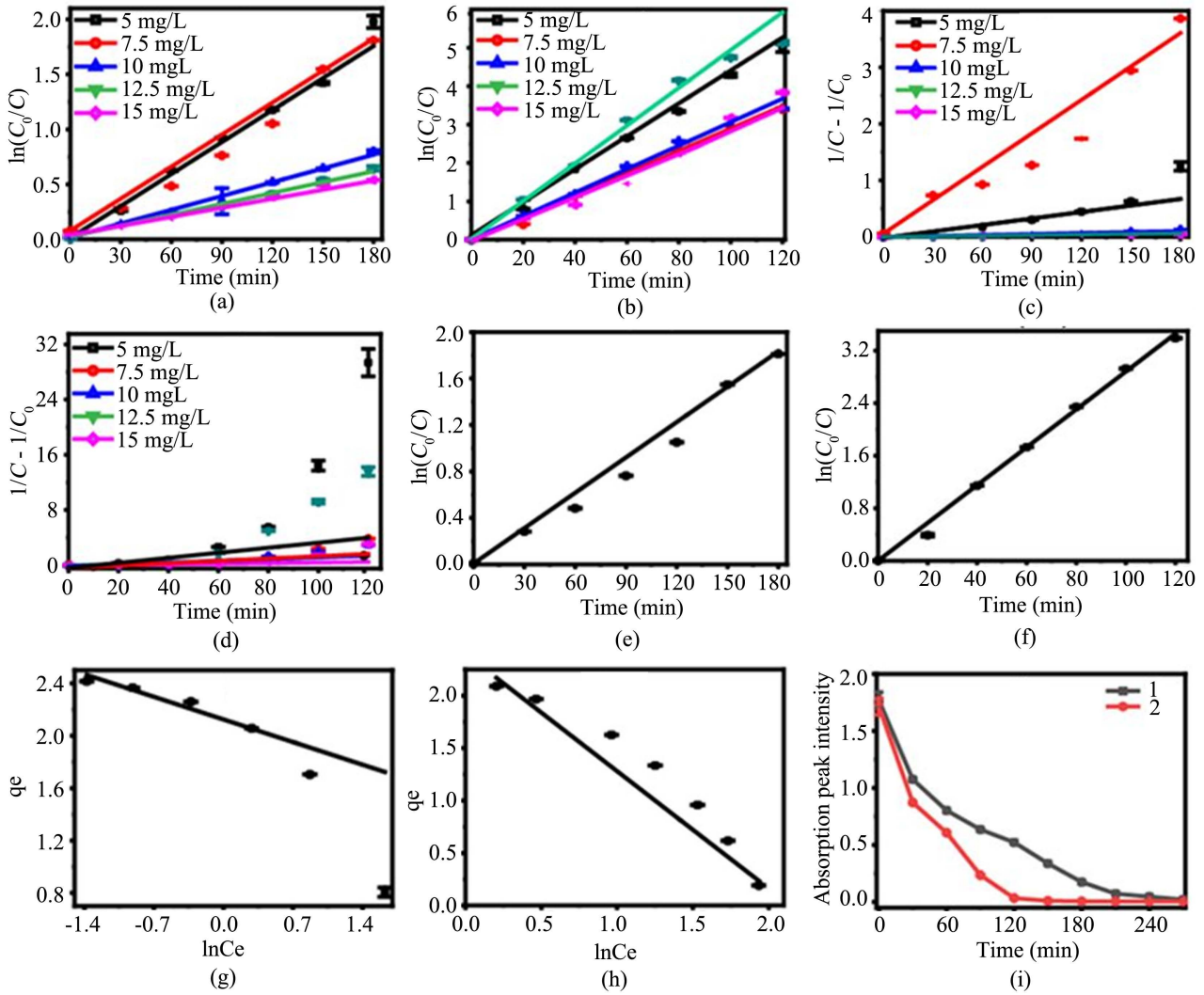

Figure 3. Degradation kinetics for ((a) and (b)) pseudo-first order and ((c) and (d)) pseudo-second order for ZnS NPs and ZnS/CDs, respectively. Adsorption models with ((e) and (f)) Langmuir-Hinshelwood and, ((g) and (h)) Temkin of MB at 7.5 mg/L over 300 mg for ZnS NPs and ZnS/CDs, respectively. (i) UHC wastewater degradation after the addition of 7.5 mg/L MB, using ZnS NPs (1) and ZnS/CDs (2) as photocatalyst.

and pseudo second order (Figure 3(c) and Figure 3(d)) in the presence of ZnS NPs and ZnS/CDs, respectively. The results of the k_1 rate constants and the different R^2 correlation coefficients are recorded in Table 1. As shown, the R^2 values are clearly closer to 1 for the pseudo first order than those obtained in the case of pseudo second order in the presence of both photocatalysts (ZnS NPs and ZnS/CDs). These results obviously indicate that the MB degradation follows apparent pseudo first-order kinetics.

Furthermore, the kinetic study of the adsorption processes gives information on the adsorption mechanism and on the mode of transfer of solutes from the liquid to the solid phase. In order to better explore this phenomenon, the study of MB isotherms on ZnS NPs and ZnS/CDs photocatalysts was also evaluated using Langmuir-Hinshelwood and Temkin isotherms (Figures 3(e)-(h)). Table 2 shows the values of the determination coefficients R^2, and the constants of the Langmuir-Hinshelwood and Temkin adsorption isotherms. In the case of the Langmuir-Hinshelwood isotherm, the R^2 are equal to 0.9995 and 0.9997 for the ZnS NPs and ZnS/CDs photocatalysts, respectively. These values are very close to 1, suggesting that the MB degradation takes place on the surface of these photocatalysts. Indeed, during the MB degradation mechanism, the molecules absorbed at the photocatalyst surface undergo a bimolecular reaction at the nearest nucleophilic sites [31]. As for Temkin isotherm, the R^2 (0.9064 and 0.9810 for ZnS NPs and ZnS/CDs, respectively) are relatively close to 1, suggests also that the heat of adsorption of all molecules decreases linearly with the increase of the adsorbent surface area. Both Langmuir-Hinshelwood and Temkin isotherms can therefore, be used to describe the adsorption of MB on these photocatalysts.

Table 1. Kinetic parameters of MB degradation.

Initial Concentration of MB (mg/L)	Pseudo-first order				Pseudo-second order	
	k_1 (min^{-1})		R^2		R^2	
	ZnS NPs	ZnS/CDs	ZnS NPs	ZnS/CDs	ZnS NPs	ZnS/CDs
5	0.0090	0.0429	0.9949	0.9984	0.9391	0.9060
7.5	0.0097	0.0492	0.9995	0.9997	0.9790	0.9730
10	0.0042	0.0306	0.9985	0.9996	0.9271	0.9710
12.5	0.0033	0.0305	0.9984	0.9987	0.8592	0.9590
15	0.0027	0.0292	0.9796	0.9963	0.7236	0.9048

Table 2. Equilibrium parameters of MB adsorption isotherms on ZnS NPs and ZnS/CDs.

Models	R^2		K_{L-H}		Lnk_t		B_1	
	a*	b*	a*	b*	a*	b*	a*	b*
Langmuir-Hinshewood	0.9995	0.9997	0.0097	0.0492	…	…	…	…
Temkin	0.9064	0.9810	…	…	−8.6116	−2.1455	−0.2467	−1.1178

a*: ZnS NPs and b*: ZnS/CDs.

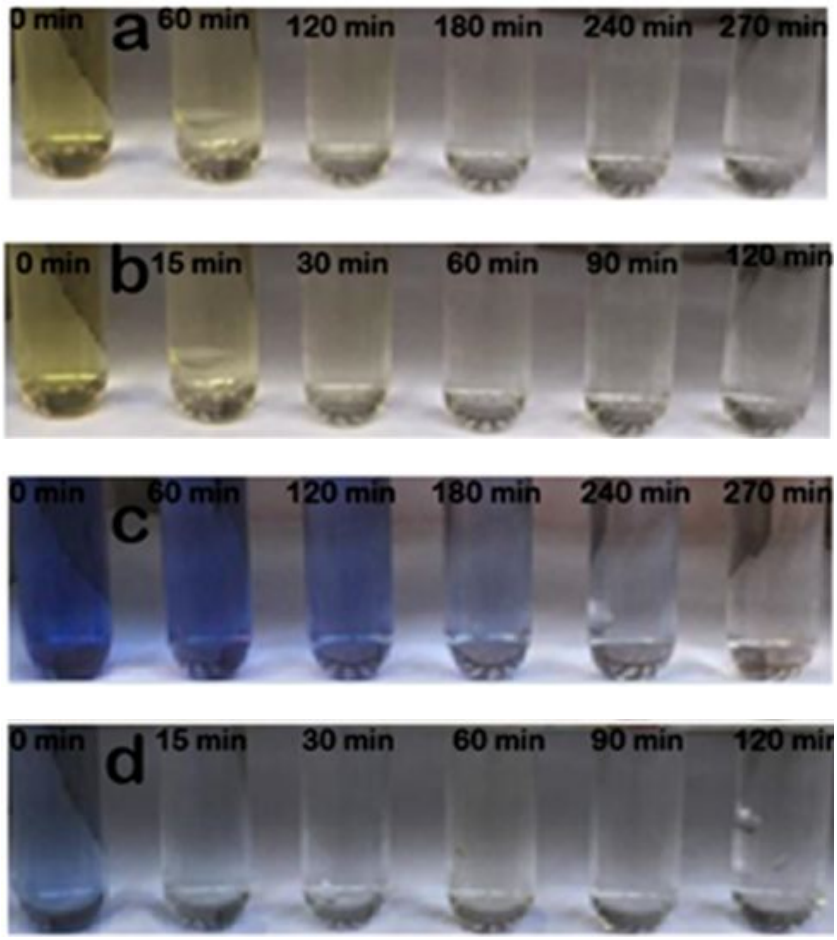

Figure 4. Images of UHCC wastewater during its degradation using (a) ZnS NPs and (b) ZnS/CDs, and UHCC wastewater contaminated with 7.5 mg/L MB during its degradation using (c) ZnS NPs and (d) ZnS/CDs.

3.3. Application

In order to study the photocatalytic activity of synthesized ZnS NPs and ZnS/CDs in a real solution, wastewater from the University Hospital Center of Cocody (UHCC) was examined. The characteristic peak around 664 nm of MB in the MB-contaminated UHCC wastewater was followed in the presence of 300 mg of ZnS NPs or ZnS/CDs photocatalysts under solar irradiation at room temperature (**Figure 3(i)**). It should be noted that after 270 min and 120 min, a complete discoloration of these wastewater samples was observed in the presence of ZnS NPs and ZnS/CDs, respectively (**Figure 4**). As displayed, this MB discoloration is faster (a short time) in the presence of ZnS/CDs in the contaminated MB wastewater, confirming that ZnS/CDs are more efficient than ZnS NPs alone.

4. Conclusion

In this work, green fluorescent carbon dots (CDs) are used to form a nanocomposite with zinc sulfide nanoparticles (ZnS/CDs). Evaluation of their photocatalytic properties indicates that the rate of MB degradation follows apparent first-order

kinetics regardless of the photocatalyst used. It was also found that the Langmuir-Hinshelwood type model best describes the degradation of MB, indicating that the chemical transformation of MB takes place at the surface of the photocatalyst. This performance may be attributed to the reduction of the reflection properties of ZnS NPs in the visible range by the presence of CDs. This ability of CDs to improve photocatalytic properties could thus allow ZnS/CDs to be ideal candidates for the degradation of organic pollutants in general and MB in particular in an aquatic environment under solar irradiation.

Conflicts of Interest

The authors declare no conflicts of interest regarding the publication of this paper.

References

[1] Velusamy, S., Roy, A., Sundaram, S. and Kumar Mallick, T. (2021) A Review on Heavy Metal Ions and Containing Dyes Removal through Graphene Oxide-Based Adsorption Strategies for Textile Wastewater Treatment. *The Chemical Record*, **21**, 1570-1610. https://doi.org/10.1002/tcr.202000153

[2] Zhao, W.-H., Wei, Z.-Q., Wu, X.-J., Zhang, X.-D., Zhang, L. and Xuan, W. (2019) Microstructure and Photocatalytic Activity of Ni-Doped ZnS Nanorods Prepared by Hydrothermal Method. *Transactions of Nonferrous Metals Society of China*, **29**, 157-164. https://doi.org/10.1016/S1003-6326(18)64924-6

[3] Avais, M. and Chattopadhyay, S. (2021) Hierarchical Porous Polymers via a Microgel Intermediate: Green Synthesis and Applications toward the Removal of Pollutants. *ACS Applied Polymer Materials*, **3**, 789-800. https://doi.org/10.1021/acsapm.0c01086

[4] Piaskowski, K., Świderska-Dąbrowska, R. and Zarzycki, P.K. (2018) Dye Removal from Water and Wastewater Using Various Physical, Chemical, and Biological Processes. *Journal of AOAC International*, **101**, 1371-1384. https://doi.org/10.5740/jaoacint.18-0051

[5] Ahmad, A., Mohd-Setapar, S.H., Chuong, C.S., Khatoon, A., Wani, W.A., Kumar, R. and Rafatullah, M. (2015) Recent Advances in New Generation Dye Removal Technologies: Novel Search for Approaches to Reprocess Wastewater. *RSC Advances*, **5**, 30801-30818. https://doi.org/10.1039/C4RA16959J

[6] Fang, X., Zhai, T., Gautam, U.K., Li, L., Wu, L., Bando, Y. and Golberg, D. (2011) ZnS Nanostructures: From Synthesis to Applications. *Progress in Materials Science*, **56**, 175-287. https://doi.org/10.1016/j.pmatsci.2010.10.001

[7] Corrado, C., Jiang, Y., Oba, F., Kozina, M., Bridges, F. and Zhang, J.Z. (2009) Synthesis, Structural, and Optical Properties of Stable ZnS: Cu, Cl Nanocrystals. *The Journal of Physical Chemistry A*, **113**, 3830-3839. https://doi.org/10.1021/jp809666t

[8] Fang, X., Bando, Y., Gautam, U.K., Zhai, T., Zeng, H., Xu, X., Liao, M. and Golberg, D. (2009) ZnO and ZnS Nanostructures: Ultraviolet-Light Emitters, Lasers, and Sensors. *Critical Reviews in Solid State and Materials Sciences*, **34**, 190-223. https://doi.org/10.1080/10408430903245393

[9] Radychev, N., Kempken, B., Krause, C., Li, J., Kolny-Olesiak, J., Borchert, H. and Parisi, J. (2015) Photovoltaic Response of Hybrid Solar Cells with Alloyed ZnS-$CuInS_2$ Nanorods. *Organic Electronics*, **21**, 92-99.

https://doi.org/10.1016/j.orgel.2015.02.027

[10] Raksha, K., Ananda, S. and Madegowda, N.M. (2015) Study of Kinetics of Photocatalysis, Bacterial Inactivation and OH Scavenging Activity of Electrochemically Synthesized Se^{4+} Doped ZnS Nanoparticles. *Journal of Molecular Catalysis A*: *Chemical*, **396**, 319-327. https://doi.org/10.1016/j.molcata.2014.10.005

[11] Kaur, M. and Nagaraja, C. (2015) Template-Free Synthesis of ZnS Nanocrystals with a New Sulfur Source and Their Photocatalytic Study. *Materials Letters*, **154**, 90-93. https://doi.org/10.1016/j.matlet.2015.04.070

[12] Bao, N., Shen, L., Takata, T. and Domen, K. (2008) Self-Templated Synthesis of Nanoporous CdS Nanostructures for Highly Efficient Photocatalytic Hydrogen Production under Visible Light. *Chemistry of Materials*, **20**, 110-117. https://doi.org/10.1021/cm7029344

[13] Tee, S.Y., Win, K.Y., Teo, W.S., Koh, L.D., Liu, S., Teng, C.P. and Han, M.Y. (2017) Recent Progress in Energy-Driven Water Splitting. *Advanced Science*, **4**, Article ID: 1600337. https://doi.org/10.1002/advs.201600337

[14] Huang, Y., Zhao, P., Miao, H., Shao, S., Wang, L., Chen, Y., Jia, C. and Xia, J. (2021) Organic-Inorganic TCPP/BiOCl Hybrids with Accelerated Interfacial Charge Separation for Boosted Photocatalytic Performance. *Colloids and Surfaces A*: *Physicochemical and Engineering Aspects*, **616**, Article ID: 126367. https://doi.org/10.1016/j.colsurfa.2021.126367

[15] Kudo, A. and Miseki, Y. (2009) Heterogeneous Photocatalyst Materials for Water Splitting. *Chemical Society Reviews*, **38**, 253-278. https://doi.org/10.1039/B800489G

[16] Reddy, D.A., Ma, R., Choi, M.Y. and Kim, T.K. (2015) Reduced Graphene Oxide Wrapped ZnS-Ag_2S Ternary Composites Synthesized via Hydrothermal Method: Applications in Photocatalyst Degradation of Organic Pollutants. *Applied Surface Science*, **324**, 725-735. https://doi.org/10.1016/j.apsusc.2014.11.026

[17] Williams, I.B.I., Kouadio Fodjo, E., Amadou, K., Albert, T. and Kong, C. (2021) Enhancing the Photocatalytic Activity of TiO_2 Nanoparticles Using Green Carbon Quantum Dots. *International Journal of Nano Dimension*, **13**, 144-154. http://www.ijnd.ir/article_685460.html

[18] Dhatshanamurthi, P., Subash, B., Senthilraja, A., Kuzhalosai, V., Krishnakumar, B. and Shanthi, M. (2014) Synthesis and Characterization of ZnS-TiO_2 Photocatalyst and Its Excellent Sun Light Driven Catalytic Activity. *Journal of Nanoscience and Nanotechnology*, **14**, 4930-4939. https://doi.org/10.1166/jnn.2014.8693

[19] Muthulingam, S., Bae, K.B., Khan, R., Lee, I.-H. and Uthirakumar, P. (2016) Carbon Quantum Dots Decorated N-Doped ZnO: Synthesis and Enhanced Photocatalytic Activity on UV, Visible and Daylight Sources with Suppressed Photocorrosion. *Journal of Environmental Chemical Engineering*, **4**, 1148-1155. https://doi.org/10.1016/j.jece.2015.06.029

[20] Kaur, S., Sharma, S. and Kansal, S.K. (2016) Synthesis of ZnS/CQDs Nanocomposite and Its Application as a Photocatalyst for the Degradation of an Anionic Dye, ARS. *Superlattices and Microstructures*, **98**, 86-95. https://doi.org/10.1016/j.spmi.2016.08.011

[21] Urbain, K.Y., Fodjo, E.K., Ardjouma, D., Serge, B.Y., Aimé, E.S., Marc, G.I. and Albert, T. (2017) Removal of Imidacloprid Using Activated Carbon Produced from *Ricinodendron heudelotii* Shells. *Bulletin of the Chemical Society of Ethiopia*, **31**, 397-409. https://doi.org/10.4314/bcse.v31i3.4

[22] Kavitha, D. and Namasivayam, C. (2007) Experimental and Kinetic Studies on Methylene Blue Adsorption by Coir Pith Carbon. *Bioresource Technology*, **98**, 14-21.

https://doi.org/10.1016/j.biortech.2005.12.008

[23] Sun, X. and Lei, Y. (2017) Fluorescent Carbon Dots and Their Sensing Applications. *TrAC Trends in Analytical Chemistry*, **89**, 163-180. https://www.sciencedirect.com/science/article/pii/S0165993616303363 https://doi.org/10.1016/j.trac.2017.02.001

[24] Lin, L. and Zhang, S. (2012) Creating High Yield Water Soluble Luminescent Graphene Quantum Dots via Exfoliating and Disintegrating Carbon Nanotubes and Graphite Flakes. *Chemical Communications*, **48**, 10177-10179. https://doi.org/10.1039/c2cc35559k

[25] Jothibas, M., Manoharan, C., Jeyakumar, S.J., Praveen, P., Punithavathy, I.K. and Richard, J.P. (2018) Synthesis and Enhanced Photocatalytic Property of Ni Doped ZnS Nanoparticles. *Solar Energy*, **159**, 434-443. https://doi.org/10.1016/j.solener.2017.10.055

[26] Murugadoss, G. and Rajesh Kumar, M. (2014) Synthesis and Optical Properties of Monodispersed Ni^{2+}-Doped ZnS Nanoparticles. *Applied Nanoscience*, **4**, 67-75. https://link.springer.com/article/10.1007/s13204-012-0167-8 https://doi.org/10.1007/s13204-012-0167-8

[27] Ming, F., Hong, J., Xu, X. and Wang, Z. (2016) Dandelion-Like ZnS/Carbon Quantum Dots Hybrid Materials with Enhanced Photocatalytic Activity toward Organic Pollutants. *RSC Advances*, **6**, 31551-31558. https://doi.org/10.1039/C6RA02840C

[28] Ouni, S., Mohamed, N.B.H., Bouzidi, M., Bonilla-Petriciolet, A. and Haouari, M. (2021) High Impact of Thiol Capped ZnS Nanocrystals on the Degradation of Single and Binary Aqueous Solutions of Industrial Azo Dyes under Sunlight. *Journal of Environmental Chemical Engineering*, **9**, Article ID: 105915. https://doi.org/10.1016/j.jece.2021.105915

[29] Goharshadi, E.K., Hadadian, M., Karimi, M. and Azizi-Toupkanloo, H. (2013) Photocatalytic Degradation of Reactive Black 5 Azo Dye by Zinc Sulfide Quantum Dots Prepared by a Sonochemical Method. *Materials Science in Semiconductor Processing*, **16**, 1109-1116. https://doi.org/10.1016/j.mssp.2013.03.005

[30] Rajabi, H.R., Sajadiasl, F., Karimi, H. and Alvand, Z.M. (2020) Green Synthesis of Zinc Sulfide Nanophotocatalysts Using Aqueous Extract of Ficus Johannis Plant for Efficient Photodegradation of Some Pollutants. *Journal of Materials Research and Technology*, **9**, 15638-15647. https://doi.org/10.1016/j.jmrt.2020.11.017 https://www.sciencedirect.com/science/article/pii/S2238785420319839

[31] Ateia, M., Alalm, M.G., Awfa, D., Johnson, M.S. and Yoshimura, C. (2020) Modeling the Degradation and Disinfection of Water Pollutants by Photocatalysts and Composites: A Critical Review. *Science of the Total Environment*, **698**, Article ID: 134197. https://doi.org/10.1016/j.scitotenv.2019.134197

Supplementary File

Calibration of residual MB detection after degradation

In order to quantitatively examine the concentration of MB remaining in the solution after degradation with 300 mg of ZnS NPs or ZnS/CDs, the calibration curve is established by plotting the absorbance peak against different MB concentration of 0.25 mg/L, 0.5 mg/L, 1 mg/L, 1.5 mg/L, 2 mg/L, 2.5 mg/L, 3 mg/L, 3.5 mg/L, 4 mg/L, 4.5 mg/L, 5 mg/L, 7.5 mg/L, 9 mg/L, 10 mg/L, 11 m/L, 12.5 mg/L, 14 mg/L, and 15 mg/L (**Figure S1**). A linear range from 0.25 mg/L to 15 mg/L as displayed in Equation (S1):

$$\Delta A = 0.032 \times C + 0.202 \quad \text{(S1)}$$

with C the concentration of MB in mg/L.

This Equation (S1) was used to evaluate the remaining concentration of MB in the solution during degradation at different times.

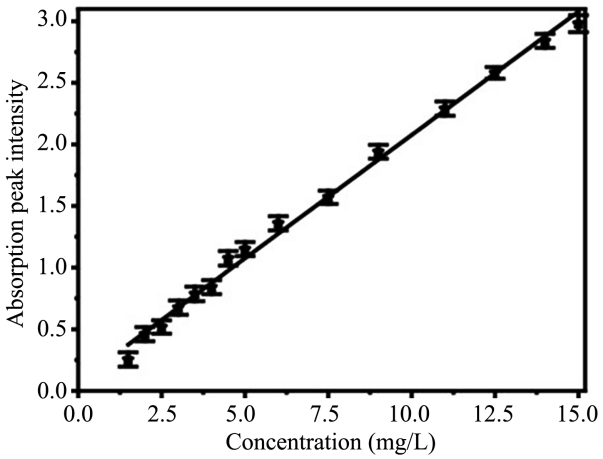

Figure S1. MB concentration calibration curve for a concentration ranging from 0.25 mg/L to 15 mg/L.